

Stochastic Resetting Accelerates Policy Convergence in Reinforcement Learning

Jello Zhou,¹ Vudtiwat Ngampruetikorn,^{2,3,*} and David J. Schwab^{4,*}

¹*Biophysics Program, Stanford University, Stanford, California 94301, USA*

²*School of Physics, University of Sydney, Sydney, NSW 2006, Australia*

³*National Institute for Theory and Mathematics in Biology,*

Northwestern University and The University of Chicago, Chicago, IL 60611, USA

⁴*Initiative for the Theoretical Sciences and Princeton-CUNY Center for the Physics of Biological Function, The Graduate Center, CUNY, New York, NY 10016, USA*

(Dated:)

Stochastic resetting, where a dynamical process is intermittently returned to a fixed reference state, has emerged as a powerful mechanism for optimizing first-passage properties. Existing theory largely treats static, non-learning processes. Here we ask how stochastic resetting interacts with reinforcement learning, where the underlying dynamics adapt through experience. In tabular grid environments, we find that resetting accelerates policy convergence even when it does not reduce the search time of a purely diffusive agent, indicating a novel mechanism beyond classical first-passage optimization. In a continuous control task with neural-network-based value approximation, we show that random resetting improves deep reinforcement learning when exploration is difficult and rewards are sparse. Unlike temporal discounting, resetting preserves the optimal policy while accelerating convergence by truncating long, uninformative trajectories to enhance value propagation. Our results establish stochastic resetting as a simple, tunable mechanism for accelerating learning, translating a canonical phenomenon of statistical mechanics into an optimization principle for reinforcement learning.

I. INTRODUCTION

Restarting a process from a reference state is among the simplest and most widespread forms of control. Foraging animals routinely return to a home base between searches [1, 2], restart strategies accelerate combinatorial optimization [3–5], and kinetic proofreading exploits repeated reversion to an unbound state to achieve molecular specificity beyond equilibrium bounds [6, 7]. Despite such ubiquity, when and why restarts improve the performance of systems that learn from experience remains poorly understood.

Stochastic resetting provides an exactly solvable framework for analyzing random restarts in stochastic processes [8–10]. For a diffusive searcher on an unbounded domain, whose mean first-passage time (MFPT) to a target is infinite, randomly resetting to a fixed position makes it finite—and minimizable. This observation has since grown into a broad theoretical program with universality results [11, 12] and extensions well beyond the original diffusive setting [13–15].

So far, resetting theory has been developed primarily for static underlying processes—that is, the searcher does not adapt based on previous trajectories. Existing extensions toward adaptive behavior are largely limited to analytically tractable settings in which the reset protocol is predefined and the underlying stochastic process remains stationary [16, 17]. Learning agents, by contrast, continually update their strategies so that the underlying process evolves and improves through experience. This interplay between resetting and learning represents a qualitatively new regime outside the scope of existing theory.

Reinforcement learning (RL) offers a natural setting to investigate this interplay [18]. An RL agent improves its

policy by interacting with an environment and updating value functions based on observed rewards. Unlike a memoryless searcher, the agent carries forward what it has learned, so resetting does not merely shorten individual trajectories—it shapes how experience accumulates across training. Resetting affects both search and learning dynamics. First, it can increase the rate at which the agent encounters rewards by discouraging long trajectories. Second, it reshapes how reward information propagates across the state space. A fundamental question arises as to which mechanism dominates and under what conditions resetting improves learning.

Here, we investigate stochastic resetting as a control parameter for reinforcement learning. Beginning with Q-learning [19]—a canonical model-free RL algorithm—in Grid-World and stochastic cliff environments, we show that resetting robustly accelerates policy convergence. It improves both search efficiency and learning speed in large environments; in smaller systems where resetting does *not* reduce the MFPT for a random walker, faster convergence persists, demonstrating that resetting accelerates learning beyond what search optimization alone would predict. To clarify the mechanism, we compare the effects of resetting with the discount factor γ . While discounting modifies the optimal value landscape and thus changes the learned policy, stochastic resetting leaves the optimal policy unchanged; instead, it biases learning toward shorter effective trajectories and more efficient reward propagation.

Moving beyond tabular settings, we consider the continuous-state MountainCar benchmark [20], solved with a Deep Q-Network (DQN) [21], which approximates the action-value function with a neural network. We vary both the exploration difficulty and the reward structure. Resetting accelerates learning when the environment poses a hard exploration problem and the primary bottleneck is finding rewards rather than propagating them to distant states. Taken together, our results establish stochastic resetting as a simple, tunable mechanism for accelerating learning in adaptive systems, opening a quanti-

* These authors contribute equally to this work.

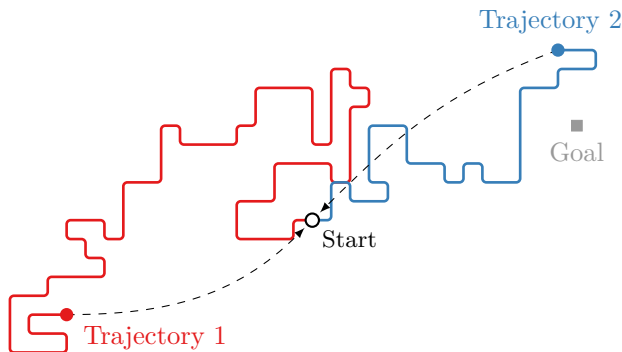


FIG. 1. **Competing effects of resetting on search efficiency.** Two trajectories (solid lines) begin at the same starting position. The first wanders away from the goal; resetting it to the starting position (dashed line) shortens the distance to the goal. The second has already moved closer to the goal; resetting it increases the distance from the goal and increases the search time. Whether resetting accelerates search on average depends on the balance between these two cases—a balance controlled by the reset rate, the environment and the underlying stochastic process.

tative connection between nonequilibrium resetting processes studied in statistical physics and the dynamics of reinforcement learning.

II. RESULTS

We study stochastic resetting in three environments of increasing complexity: a tabular GridWorld, a stochastic cliff environment (WindyCliff) and the continuous-state Mountain-Car solved with a Deep Q-Network. In each case, resetting is implemented as an external intervention. At every training step, the agent returns to the start state with probability r , regardless of the agent’s action and current state. Since interactions with the environment dominate the cost of RL, we use the cumulative number of training steps across episodes (i.e., the number of times the agent interacts with the environment) as our measure of sample efficiency. Performance is evaluated every 1000 training steps by running a greedy episode with resetting and exploration turned off. Resetting does not affect the learned value function (Q-table or neural network); it modifies only the distribution of training trajectories while preserving all accumulated knowledge. Full algorithmic and hyperparameter details are provided in Materials and Methods.

A. Resetting accelerates policy convergence beyond search optimization

Stochastic resetting accelerates policy convergence in GridWorld, and the benefit persists even when resetting does not improve search efficiency. We compare two grid sizes: $N = 120$, where resetting reduces the median first-passage time (FPT) of a random walker to the goal, and $N = 60$, where it does not, see Fig. 2B (dashed curves). We focus here on the median statistic

rather than the mean because it is more stable in the presence of outliers and better captures the behavior of a typical RL agent. Since the median is less sensitive to heavy tails than the mean, resetting reduces the median FPT only in sufficiently difficult search problems whose FPT distributions are heavy-tailed enough [22]. These two regimes allow us to isolate the contributions of search efficiency (how quickly the agent first encounters the goal) from learning speed (how quickly value information propagates to yield a good policy).

For a large grid ($N = 120$), resetting speeds up both search and policy convergence. At every training step, a finite resetting probability, $r > 0$, results in shorter evaluation episodes, Fig. 2A. The dependence on r differs between search and learning. The median FPT has a clear optimum near $r \sim 10^{-3}$, whereas the training steps needed for convergence decrease monotonically with any nonzero r , Fig. 2B. In particular, $r = 0$ performs substantially worse than every nonzero reset rate across all exploration rates ε tested. This separation suggests that resetting accelerates learning beyond what search improvement alone would predict.

In the smaller system ($N = 60$), resetting worsens search. The median FPT increases monotonically with r . At early training stages the ordering of evaluation curves reflects this search penalty—larger r leads to longer episodes. However, the $r = 0.0015$ curve drops below the $r = 0$ curve, indicating faster policy convergence despite worse search, Fig. 2A. The magnitude of this benefit depends on the exploration rate. Resetting accelerates convergence for moderate values ($\varepsilon = 0.1$ and 0.5) but not for highly exploratory agents ($\varepsilon = 0.9$), which behave similarly to random walkers and are therefore dominated by the search penalty, Fig. 2B.

The learning benefit of resetting can be traced to how it reshapes the trajectories along which reward information propagates. In one-step temporal-difference algorithms such as Q-learning, value information spreads backward from the goal (through successive Bellman updates) [18, 19]. Each visit to the goal updates only the immediately preceding state and repeated visits gradually propagate value toward earlier states. The speed of this process depends on the length and directness of the trajectories. Resetting truncates long, indirect exploratory paths, so goal-reaching episodes tend to consist of shorter segments between the final reset-to-start and the goal (Fig. 2C), resulting in faster policy convergence. Q-table snapshots confirm this picture: at fixed ε , increasing r causes the learned value function to propagate along progressively more direct routes (Fig. 12). For some values of ε , Q-values corresponding to actions from the start that move away from the goal remain largely unpopulated, indicating that value propagation does not occur along strongly meandering paths.

When resetting also improves search ($N = 120$), both mechanisms are at play and the speedup is large. When resetting decelerates search ($N = 60$), the learning mechanism can still dominate at moderate exploration rates, resulting in a net benefit. At high ε the agent’s behavior approaches that of a random walker, search effects dominate and resetting becomes detrimental.

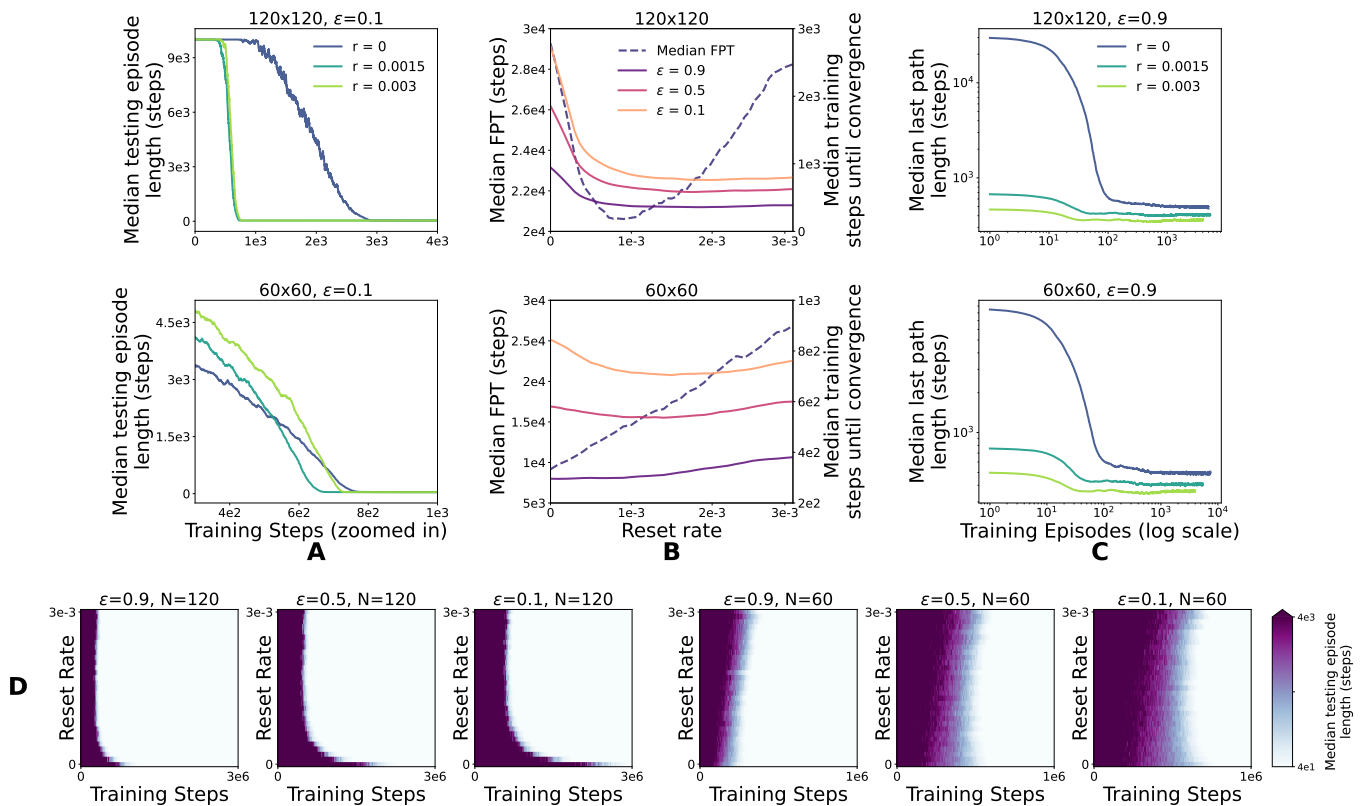


FIG. 2. **Learning dynamics in GridWorld.** (A) Median evaluation episode length during training for grid sizes $N = 120$ and $N = 60$, shown for reset rates $r = 0, 0.0015$, and 0.003 (250 trials per condition). Plots are zoomed in to regions where learning dynamics are most prominent. (B) Separation of search and learning effects. Dashed curves (left axis): numerically computed median first-passage time (FPT) of a random walker, averaged over 2500 trials. Solid curves (right axis): median number of training steps until evaluation episode length converges to its optimum of 40 steps, shown for three exploration rates ϵ . (C) Evolution of the final contiguous path from the last reset to the goal over training episodes. (D) Heatmaps of median evaluation episode length as a function of reset rate and training steps (colour bar capped at 4000 steps). Full training, testing, and last-path curves are shown in Figs. 10, 11.

B. Resetting modifies training dynamics without changing the optimal policy

A natural question is whether stochastic resetting provides functionality distinct from the discount factor γ , the standard reinforcement learning parameter that controls how strongly future rewards are weighted. The WindyCliff environment—a stochastic cliff task in which wind blows the agent downward with probability p_w , see Fig. 5b—offers a clean test since its optimal policy is sensitive to γ . Smaller γ values discount the distant goal reward relative to the immediate cliff penalty, favoring longer, cliff-avoidant paths, while larger γ favors shorter, riskier ones. Bellman iterations confirm that the dynamic-programming optimal path length $L^*(\gamma)$ decreases with γ , Fig. 3F. Dynamically, smaller γ values produce a larger region of negative Q -values adjacent to the cliff during Q -learning, consistent with cliff-avoidant behavior (Fig. 14). The discount factor therefore reshapes the optimal policy itself.

Resetting behaves differently. At fixed $\gamma = 0.98$, varying the reset rate shifts the speed of convergence but not its endpoint. Agents with different resetting rates converge to the same final episode length, Fig. 3A and D. Conversely, varying γ at

fixed $r = 0$ yields similar convergence rates but different final policies, each matching its respective $L^*(\gamma)$, Fig. 3B and E.

These results establish a fundamental distinction. Discount factors reshape the optimal policy itself, whereas stochastic resetting leaves the optimal policy unchanged but can accelerate convergence by modifying training trajectories.

C. Resetting can accelerate DQN learning

To investigate stochastic resetting beyond tabular settings, we turn to the Deep Q-Network (DQN) algorithm [21] applied to the MountainCar environment [20], a continuous-state benchmark in which an underpowered car must escape a valley by building momentum (Fig. 4A). Two modifications allow us to vary the exploration difficulty and reward structure independently. First, the left boundary is set to either -1.2 (standard) or -1.7 (extended); the latter introduces a deep trap that requires specific action sequences to escape, making unassisted goal discovery substantially harder. Second, we compare a sparse positive reward ($+1$ at the goal, 0 otherwise) with a step penalty (-1 per step, 0 at the goal). The initial state is fixed at the

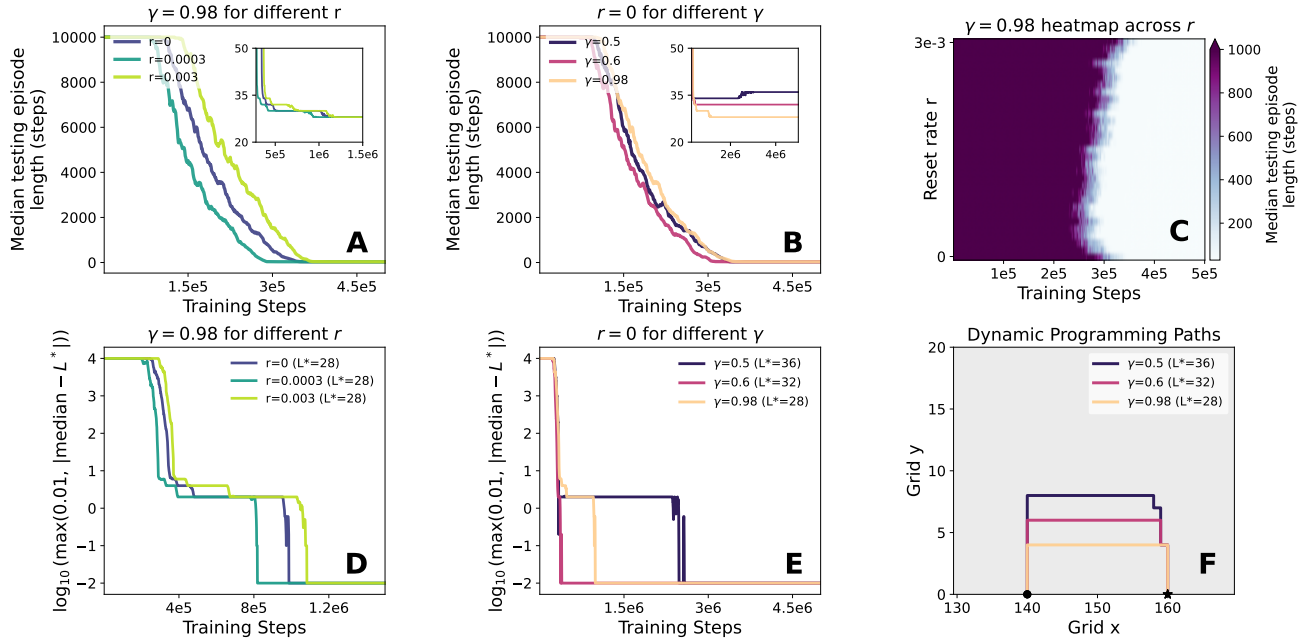


FIG. 3. **Learning dynamics in WindyCliff.** (A) Median evaluation episode length at $\gamma = 0.98$ for reset rates $r = 0, 0.0003$, and 0.003 (250 trials per condition). Inset: extended view to 1.5×10^6 training steps. (B) Learning curves at $r = 0$ for $\gamma = 0.5, 0.6$, and 0.98 . (C) Heatmap of median evaluation episode length over reset rates and training steps (capped at 1000). (D) Approach of evaluation episode length toward dynamic-programming (DP) optimal path length $L^*(\gamma)$ at $\gamma = 0.98$ for varying r . (E) Same approach for $r = 0$ and varying γ . (F) DP-optimal paths from start to goal for three values of γ . These results are for grid width 300, height 150, $p_w = 0.005$, $s_w = 3$. Full training, testing (including cliff falls), and last-path curves are shown in Fig. 13.

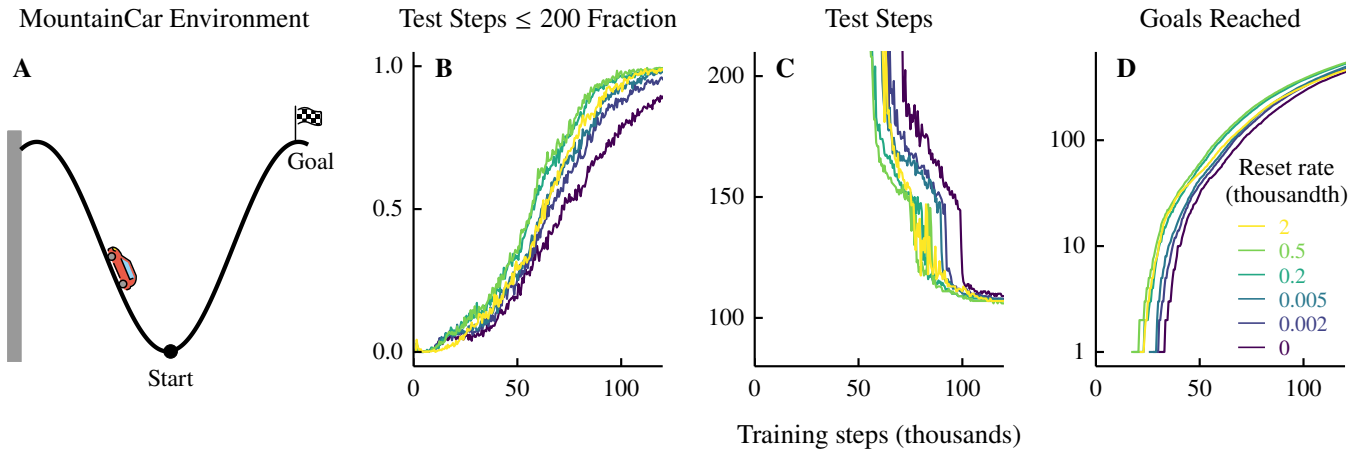


FIG. 4. **Stochastic resetting accelerates deep reinforcement learning.** (A) Schematic of the MountainCar environment: an underpowered car starting at the valley bottom must build momentum to reach the goal (flag). The left boundary is extended to -1.7 , creating a deep trap that makes unassisted goal discovery difficult. (B) Fraction of replicates achieving evaluation performance ≤ 200 steps as a function of cumulative training steps for a range of reset rates (see legend). We see that intermediate reset rates accelerate learning relative to the no-resetting baseline. (C) Median evaluation steps to goal. (D) Median cumulative number of goals reached during training. Intermediate reset rates increase the rate at which the agent encounters the goal, but excessively high rates are counterproductive. In all panels, increasing the reset rate from zero initially improves performance; beyond an intermediate optimum, further increases degrade it. The results are for the sparse reward scheme (i.e., reward is $+1$ upon reaching the goal and zero otherwise) and 512 replicates for each reset rate.

valley bottom (position, velocity) = $(-0.5, 0)$. Full details are provided in Materials and Methods.

In the extended environment under the sparse reward scheme, intermediate reset rates accelerate learning. The fraction of replicates achieving evaluation steps ≤ 200 rises earlier and stays higher compared to the no-resetting baseline (Fig. 4B), and median evaluation steps drop faster (Fig. 4C). The mechanism is visible in the training dynamics. Resetting increases the rate at which the agent encounters the goal (Fig. 4D), truncating unproductive excursions deep into the extended valley and returning the agent to the informative region near the goal. Too-high reset rates, however, interrupt trajectories so frequently that the agent cannot build the momentum needed to reach the goal, impairing both the encounter rate and learned policy.

Under the step penalty scheme, learning dynamics change qualitatively. The penalty provides a gradient signal on every transition regardless of whether the agent reaches the goal; as a result, exploration is no longer the primary bottleneck. Accordingly, learning curves for different reset rates largely overlap, and the largest rates modestly impair performance (Fig. 15). When the left boundary is set to its standard value (-1.2) , the valley is shallow enough that the agent reliably discovers the goal without assistance; resetting offers no benefit under either reward scheme (Figs. 16 and 17).

These results demonstrate that stochastic resetting accelerates deep RL when the environment poses a hard exploration problem and the reward structure is such that exploration—rather than credit assignment—is the dominant bottleneck.

III. DISCUSSION

We demonstrate that stochastic resetting accelerates reinforcement learning across all three settings considered. Resetting truncates long exploratory paths, concentrating policy updates along more direct trajectories and speeding the propagation of reward information through the state space. In GridWorld, we find that a nonzero resetting rate improves policy convergence even when it worsens diffusive search efficiency. In WindyCliff, our results show that resetting controls convergence speed without altering the learned policy—a mechanism fundamentally distinct from the discount factor, which reshapes the policy itself. In continuous-state MountainCar with deep Q-networks, we show that resetting accelerates learning when exploration is difficult and rewards are sparse. Across all environments, resetting is most beneficial when long, uninformative trajectories are the primary bottleneck. Taken together, our results establish stochastic resetting as a tunable control mechanism for reinforcement learning, connecting the nonequilibrium resetting processes studied in statistical physics to the dynamics of learning in adaptive systems.

Existing stochastic resetting theory addresses static processes in which the underlying dynamics do not change between resets [8, 9, 12]. A learning agent, by contrast, iteratively improves its strategy with experience, so the underlying process that resetting interrupts is nonstationary. Our results reveal a new mechanism through which resetting enhances learning; it shortens the chains of states along which temporal-difference

updates propagate reward information. The separation of search efficiency from learning performance in Fig. 2B directly validates this mechanism.

Stochastic resetting differs from existing approaches that seek to accelerate reinforcement learning through intrinsic reward bonuses, uncertainty-driven exploration, temporally persistent actions or mechanisms that return agents to previously visited states before expanding outward [23–28]. Resetting acts instead on the temporal structure of experience, requiring only a single control parameter. This simplicity also limits its scope: in environments with deceptive rewards or partial observability, where progress relies on identifying informative behaviors rather than abandoning unproductive trajectories, richer exploration methods remain necessary. This simplicity also limits its scope. When progress relies on identifying informative behaviors rather than abandoning unproductive trajectories, such as in environments with deceptive rewards or partial observability, richer exploration methods remain necessary.

Throughout this work, we study the memoryless stochastic resetting protocol. Its deterministic limit is fixed-interval restarting [12, 29], which is closely related to episode-length truncation, a common practical heuristic in reinforcement learning [30]. A systematic empirical comparison between stochastic and deterministic restart schedules is an important direction for future work.

Several directions remain open. In policy-gradient methods, where updates depend on entire trajectory returns rather than single-step Bellman backups (see, e.g., Ref. [31]), resetting would alter the variance and bias of gradient estimates in ways yet to be characterized. In multi-agent settings (see, e.g., Ref. [32]), shorter effective trajectories could reduce the exploration burden in combinatorially large state-action spaces. Beyond artificial agents, biological systems appear to exploit restart-like mechanisms across scales—from central-place foraging [1] and novelty-induced resets in neural systems during learning [33], to molecular error-correction via kinetic proofreading, in which an energy-consuming process returns incorrect substrates to an unbound reference state [6, 7, 34, 35]. Developing models that incorporate the physical costs and partial information characteristic of these systems would help determine whether the optimality principles identified in this work generalize to natural learning.

IV. MATERIALS AND METHODS

A. Tabular grid environments

We study two grid-based environments with discrete state and action spaces (Fig. 1).

First the ‘GridWorld’ environment is a square $N \times N$ lattice ($N \in \{60, 120\}$) with no obstacles and no stochasticity. The start and goal states are placed at $(N/2 - 10, N/2 - 10)$ and $(N/2 + 10, N/2 + 10)$, respectively, separated by a Manhattan distance of 40. The reward is +1 upon reaching the goal and zero otherwise. Actions that would move the agent outside the grid are clipped. The optimal policy corresponds to any

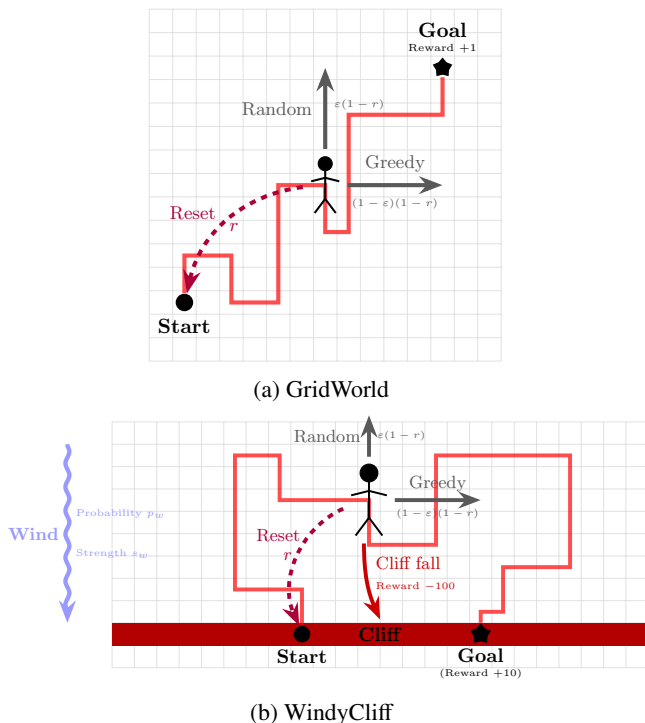


FIG. 5. Schematic of the tabular GridWorld and WindyCliff environments. In both settings the agent navigates a grid, learning via Q learning to find the shortest path from the start to the goal. At every training step the agent resets to the start with probability r and otherwise follows the standard ϵ -greedy policy. In GridWorld the agent receives reward +1 at the goal and zero otherwise. In WindyCliff the goal reward is +10 and cliff falls incur a -100 penalty; optional stochastic wind blows the agent downward s_w steps with probability p_w .

shortest path between the two states.

Second, the ‘WindyCliff’ environment is a rectangular grid of width W and height H ($W = 300$, $H = 150$ in the main experiments). The start and goal states lie on the bottom row at columns $W/2 - 10$ and $W/2 + 10$. All other bottom-row cells form a cliff. This environment is adapted from the standard Gymnasium CliffWalking environment [36], in which the start and goal states lie at the bottom corners. By increasing the distance between the start/goal and the grid edges, we can control the extent to which the agent can wander in the wrong direction and tune whether resetting reduces the first-passage time of a random agent (Fig. 9).

Stepping onto any cliff cell incurs a -100 penalty and immediately returns the agent to the start (this teleportation is non-terminal and distinct from stochastic resetting). Reaching the goal yields a reward of +10; all other transitions yield zero reward. Stochastic wind blows the agent downward by s_w cells with probability p_w at each step, encouraging cliff-avoidant routes. In the main experiments, $p_w = 0.005$ and $s_w = 3$.

Both environments use tabular Q-learning with an ϵ -greedy exploration policy. The action-value function $Q(s, a)$ is initial-

ized to zero and updated after each transition,

$$Q(s, a) \leftarrow Q(s, a) + \alpha \left[r_t + \gamma \max_{a'} Q(s', a') - Q(s, a) \right], \quad (1)$$

where α is the learning rate and γ the discount factor [18, 19]. At each training step the agent takes a uniformly random action with probability ϵ and the greedy action $\arg \max_a Q(s, a)$ otherwise. Training episodes begin at the start state and terminate upon reaching the goal. The learning rate α is linearly annealed during training to stabilize convergence, with a floor of 10^{-3} ; the exploration rate ϵ is similarly annealed with a floor of 10^{-3} , except where ϵ is held fixed for parameter sweeps.

Every 1000 training steps, the greedy policy ($\epsilon = 0$, $r = 0$) is evaluated on a separate environment instance. The recorded metric is the evaluation episode length (steps to goal). Each condition is replicated across 250 independent trials; we report medians unless otherwise stated.

B. MountainCar environment

The dynamics follow the standard Gymnasium MountainCar specification [36], with two modifications. First, the initial state is fixed at (position, velocity) = $(-0.5, 0)$ rather than a uniform random position in $[-0.6, -0.4]$. Second, the left boundary is set to either -1.2 (standard) or -1.7 (extended), the latter creating a deep trap that makes unassisted goal discovery harder. We consider two reward schemes: sparse positive (+1 at the goal, 0 otherwise) and step penalty (-1 per step, 0 at the goal).

We use DQN [21] with a two-hidden-layer multilayer perceptron (256 units per layer with ReLU activations) mapping the two-dimensional observation (position, velocity) to Q-values for three actions. Training uses experience replay with buffer size 10,000, a target network with periodic hard updates, smooth L_1 loss, and the Adam optimizer [37]. Exploration follows an ϵ -greedy schedule with ϵ linearly annealed from 1.0 to ϵ_{end} over the first 20% of training steps. The batch size is 128, learning starts at 1,000 steps, training frequency is every 16 steps, with 8 gradient steps per update, and discount factor $\gamma = 0.98$. For the sparse positive reward scheme, the learning rate is 10^{-4} , $\epsilon_{\text{end}} = 0.1$ and the target network update interval is 400. For the step penalty reward scheme, the learning rate is 4×10^{-3} , $\epsilon_{\text{end}} = 0.07$ and the target network update interval is 600. These hyperparameters are fine-tuned for each reward scheme for learning without resetting.

Each run lasts 150,000 steps. Every 500 steps, the greedy policy is evaluated on a separate environment instance with a 10,000-step horizon; the metric is steps to goal. We report the statistics over 512 independent replicates.

C. Stochastic resetting protocol

Stochastic resetting is implemented identically across all environments. At each training step, before action selection,

the agent is returned to the designated start state with a probability fixed throughout training, independent of the agent's chosen action and current state. No value-function update is performed on the reset transition itself: the Q-table (or neural network weights) persists across resets, so resetting modifies only the distribution of training trajectories while preserving all accumulated knowledge. In the MountainCar experiments, reward targets stored in the replay buffer are computed from the underlying (non-reset) transition to avoid introducing spurious value estimates.

Because resetting does not alter the reward structure or the definition of the value function, it does not change the optimal policy. Instead, it modifies exploration dynamics by truncating trajectories and increasing the frequency with which the agent revisits states near the start.

For the random-walker first-passage time baselines (Fig. 2B), we simulate a uniformly random agent on the grid with stochastic resetting and record the first-passage time to the goal across 2,500 independent trials per (N, r) pair. Full first-passage sweep results for GridWorld and WindyCliff are provided in Figs. 7-9.

D. Dynamic programming baselines

For the WindyCliff environment, we compute the optimal value function $Q^*(s, a)$ and policy $\pi^*(s)$ by iterating a Bellman equation, using the same transition and reward model as the

training environment (including stochastic wind). At each iteration,

$$Q_{k+1}(s, a) = \mathbb{E} \left[r(s, a, s') + \gamma \max_{a'} Q_k(s', a') \right], \quad (2)$$

where the expectation is over stochastic wind outcomes. Iteration proceeds until the maximum change in the value function falls below 10^{-12} . The optimal path length $L^*(\gamma)$ reported in Fig. 3F is obtained by rolling out π^* from the start state. A broader exploration of how different hyperparameters influence L^* is provided in Fig. 6.

ACKNOWLEDGMENTS

JZ acknowledges funding from Stanford University through the Graduate Program in Biophysics. VN acknowledges research funds from the University of Sydney. The research of VN was supported in part by grants from the NSF (DMS-2235451) and Simons Foundation (MPS-NITMB-00005320) to the NSF-Simons National Institute for Theory and Mathematics in Biology (NITMB). DJS was partially supported by a Simons Fellowship in the MMLS, a Sloan Fellowship, and the National Science Foundation, through the Center for the Physics of Biological Function (PHY-1734030). VN and DJS also acknowledge funding from Coefficient Giving.

-
- [1] G. H. Orions and N. E. Pearson, On the theory of central place foraging (Ohio State University Press, Columbus, 1979) pp. 154–177.
 - [2] V. Lecheval, E. J. H. Robinson, and R. P. Mann, Random walks with spatial and temporal resets can explain individual and colony-level searching patterns in ants, *J. R. Soc. Interface* **21**, 20240149 (2024).
 - [3] M. Luby, A. Sinclair, and D. Zuckerman, Optimal speedup of las vegas algorithms, *Information Processing Letters* **47**, 173–180 (1993).
 - [4] C. P. Gomes, B. Selman, and H. A. Kautz, Boosting combinatorial search through randomization, in *AAAI/IAAI* (1998).
 - [5] A. Montanari and R. Zecchina, Optimizing searches via rare events, *Phys. Rev. Lett.* **88**, 178701 (2002).
 - [6] J. J. Hopfield, Kinetic proofreading: A new mechanism for reducing errors in biosynthetic processes requiring high specificity, *Proceedings of the National Academy of Sciences* **71**, 4135 (1974).
 - [7] J. Ninio, Kinetic amplification of enzyme discrimination, *Biochimie* **57**, 587 (1975).
 - [8] M. R. Evans and S. N. Majumdar, Diffusion with stochastic resetting, *Phys. Rev. Lett.* **106**, 160601 (2011).
 - [9] M. R. Evans, S. N. Majumdar, and G. Schehr, Stochastic resetting and applications, *Journal of Physics A: Mathematical and Theoretical* **53**, 193001 (2020).
 - [10] S. Gupta and A. M. Jayannavar, Stochastic resetting: A (very) brief review, *Frontiers in Physics* **10**, 10.3389/fphy.2022.789097 (2022).
 - [11] S. Reuveni, Optimal stochastic restart renders fluctuations in first passage times universal, *Phys. Rev. Lett.* **116**, 170601 (2016).
 - [12] A. Pal and S. Reuveni, First passage under restart, *Phys. Rev. Lett.* **118**, 030603 (2017).
 - [13] L. Kusmierz, S. N. Majumdar, S. Sabhapandit, and G. Schehr, First order transition for the optimal search time of lévy flights with resetting, *Phys. Rev. Lett.* **113**, 220602 (2014).
 - [14] P. C. Bressloff, Search processes with stochastic resetting and multiple targets, *Phys. Rev. E* **102**, 022115 (2020).
 - [15] D. Gupta, C. A. Plata, A. Kundu, and A. Pal, Stochastic resetting with stochastic returns using external trap, *Journal of Physics A: Mathematical and Theoretical* **54**, 025003 (2020).
 - [16] T. D. Keidar, O. Blumer, B. Hirshberg, and S. Reuveni, Adaptive resetting for informed search strategies and the design of non-equilibrium steady-states, *Nature Communications* **16**, 7259 (2025).
 - [17] A. Falcón-Cortés, D. Boyer, L. Giuggioli, and S. N. Majumdar, Localization transition induced by learning in random searches, *Phys. Rev. Lett.* **119**, 140603 (2017).
 - [18] R. Sutton and A. Barto, Reinforcement learning: An introduction, *IEEE Transactions on Neural Networks* **9**, 1054–1054 (1998).
 - [19] C. J. C. H. Watkins and P. Dayan, Q-learning, *Machine Learning* **8**, 279–292 (1992).
 - [20] A. W. Moore, *Efficient Memory-based Learning for Robot Control*, Tech. Rep. (University of Cambridge, 1990).
 - [21] V. Mnih, K. Kavukcuoglu, D. Silver, A. A. Rusu, J. Veness, M. G. Bellemare, A. Graves, M. Riedmiller, A. K. Fidjeland, G. Ostrovski, S. Petersen, C. Beattie, A. Sadik, I. Antonoglou, H. King, D. Kumaran, D. Wierstra, S. Legg, and D. Hassabis,

- Human-level control through deep reinforcement learning, *Nature* **518**, 529 (2015).
- [22] S. Belan, Median and mode in first passage under restart, *Phys. Rev. Res.* **2**, 013243 (2020).
- [23] Y. Burda, H. Edwards, A. Storkey, and O. Klimov, *Exploration by random network distillation* (2018).
- [24] A. Ecoffet, J. Huizinga, J. Lehman, K. O. Stanley, and J. Clune, First return, then explore, *Nature* **590**, 580–586 (2021).
- [25] B. Eysenbach, A. Gupta, J. Ibarz, and S. Levine, *Diversity is all you need: Learning skills without a reward function* (2018).
- [26] I. Osband, C. Blundell, A. Pritzel, and B. Van Roy, *Deep exploration via bootstrapped dqn* (2016).
- [27] D. Pathak, D. Gandhi, and A. Gupta, *Self-supervised exploration via disagreement* (2019).
- [28] J.-B. Mouret and J. Clune, *Illuminating search spaces by mapping elites* (2015).
- [29] U. Bhat, C. De Bacco, and S. Redner, Stochastic search with poisson and deterministic resetting, *Journal of Statistical Mechanics: Theory and Experiment* **2016**, 083401 (2016).
- [30] F. Pardo, A. Tavakoli, V. Levдик, and P. Kormushev, Time limits in reinforcement learning, in *Proceedings of the 35th International Conference on Machine Learning*, Proceedings of Machine Learning Research, Vol. 80, edited by J. Dy and A. Krause (PMLR, 2018) pp. 4045–4054.
- [31] R. J. Williams, Simple statistical gradient-following algorithms for connectionist reinforcement learning, *Machine Learning* **8**, 229 (1992).
- [32] D. Strouse, M. Kleiman-Weiner, J. Tenenbaum, M. Botvinick, and D. J. Schwab, Learning to share and hide intentions using information regularization, in *Advances in Neural Information Processing Systems*, Vol. 31, edited by S. Bengio, H. Wallach, H. Larochelle, K. Grauman, N. Cesa-Bianchi, and R. Garnett (Curran Associates, Inc., 2018).
- [33] A. J. Park, A. Z. Harris, K. M. Martyniuk, C.-Y. Chang, A. I. Abbas, D. C. Lowes, C. Kellendonk, J. A. Gogos, and J. A. Gordon, Reset of hippocampal–prefrontal circuitry facilitates learning, *Nature* **591**, 615 (2021).
- [34] R. Ravasio, K. Husain, C. G. Evans, R. Phillips, M. Ribezzi-Crivellari, J. W. Szostak, and A. Murugan, Evolution of error correction through a need for speed, *Science* **391**, 818–824 (2026).
- [35] T. Rotbart, S. Reuveni, and M. Urbakh, Michaelis-menten reaction scheme as a unified approach towards the optimal restart problem, *Phys. Rev. E* **92**, 060101 (2015).
- [36] M. Towers, A. Kwiatkowski, J. U. Balis, G. D. Cola, T. Deleu, M. Goulão, K. Andreas, M. Krimmel, A. KG, R. D. L. Perez-Vicente, J. K. Terry, A. Pierré, S. V. Schulhoff, J. J. Tai, H. Tan, and O. G. Younis, Gymnasium: A standard interface for reinforcement learning environments, in *The Thirty-ninth Annual Conference on Neural Information Processing Systems Datasets and Benchmarks Track* (2025).
- [37] D. P. Kingma and J. Ba, Adam: A method for stochastic optimization, in *3rd International Conference on Learning Representations, ICLR 2015, San Diego, CA, USA, May 7-9, 2015, Conference Track Proceedings*, edited by Y. Bengio and Y. LeCun (2015).

V. SUPPLEMENTARY INFORMATION

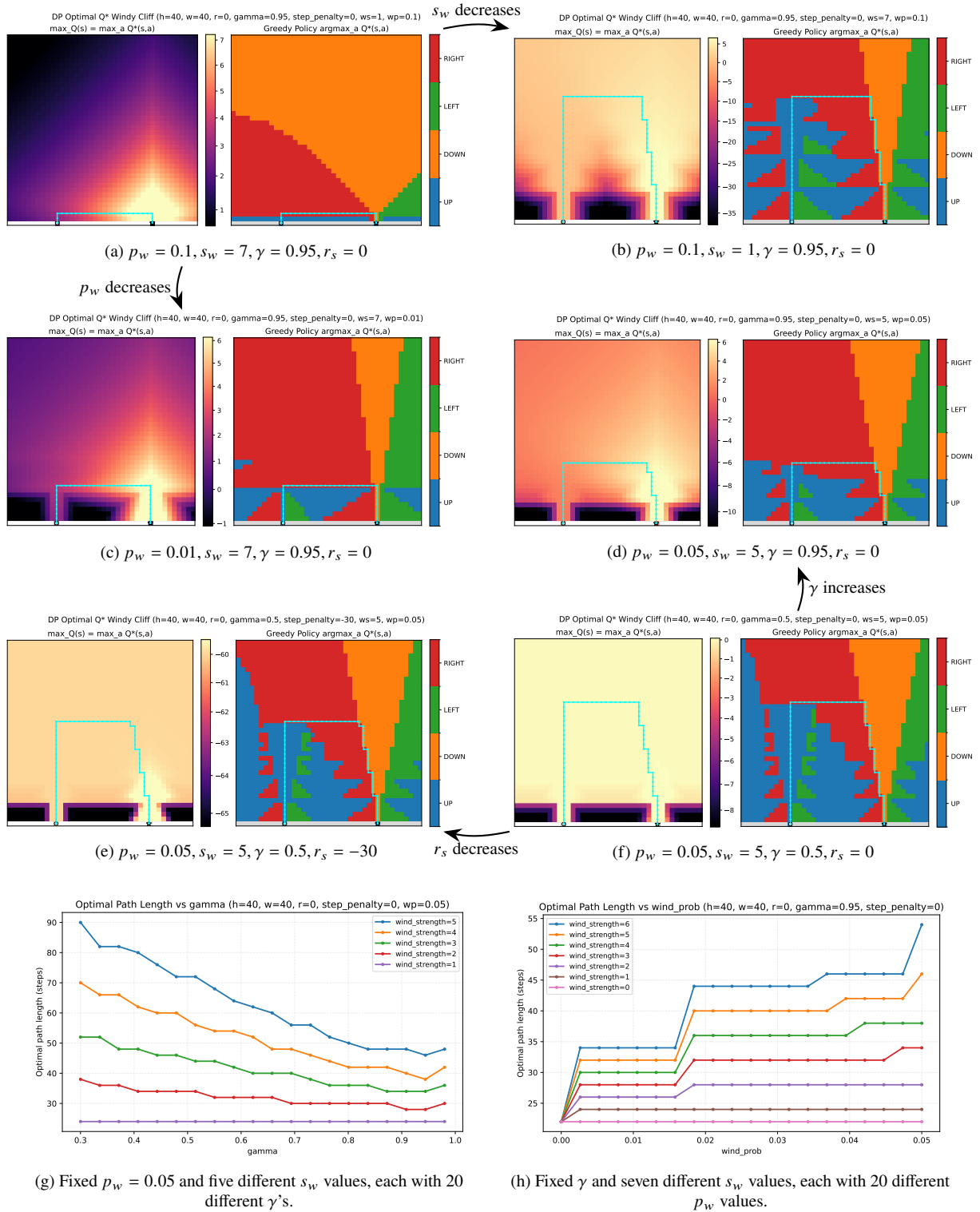
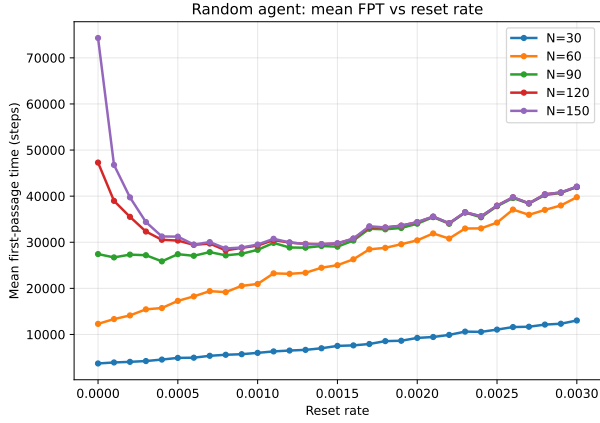
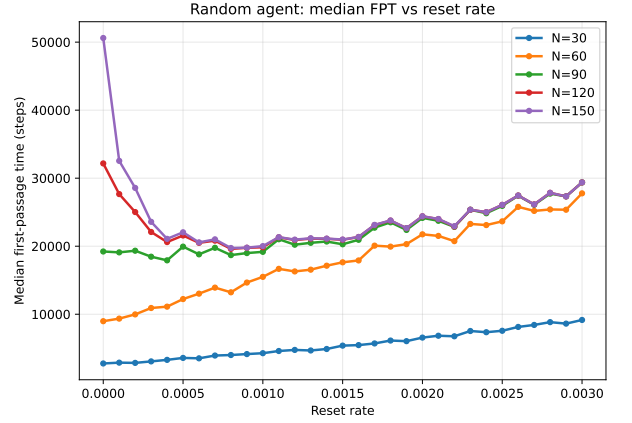


FIG. 6. (a)-(f): Heatmaps for $\max_a Q(s, a)$ for a 40×40 WindyCliff setup and corresponding greedy action maps encoding per-state greedy policies, for changing wind strengths s_w , wind probabilities p_w , discount factors γ , and step penalties r_s . The resulting optimal path is shown over both plots. (g) & (h): Optimal path lengths L^* across different γ , s_w , and p_w .

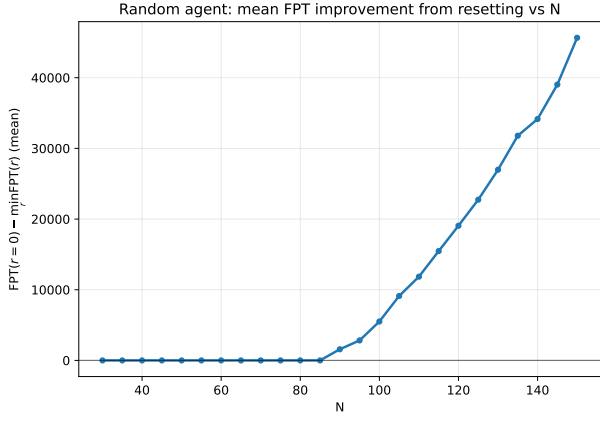
A. First-passage time distributions



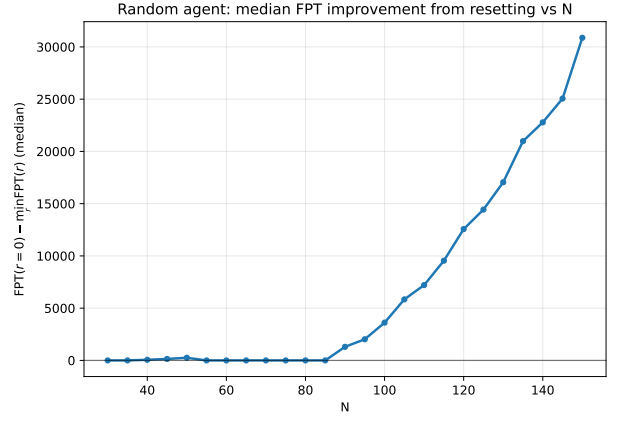
(a) Mean FPT versus reset rate for selected N .



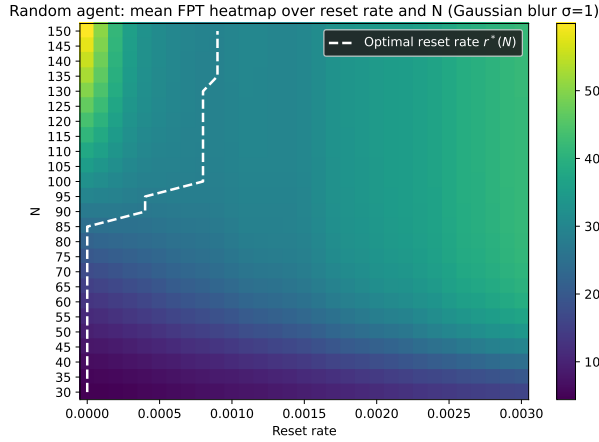
(b) Median FPT versus reset rate for selected N .



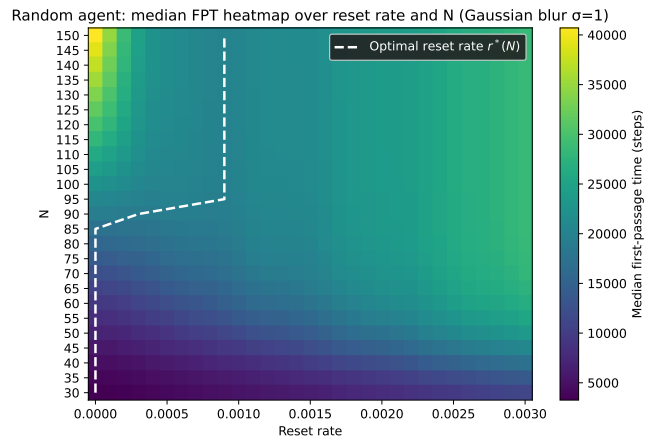
(c) Mean difference between the minimum FPT across reset rates and $FPT(r)$.



(d) Median difference between the minimum FPT across reset rates and $FPT(r)$.



(e) Heatmap of mean



(f) Heatmap of median

FIG. 7. Mean and median first-passage time statistics for GridWorld settings with varying N . Statistics are aggregated over 2500 trials. The heatmap plots are postprocessed with a Gaussian blur of $\sigma = 1$ grid space and the curve of reset rates that minimizes FPT for a given N is plotted with a dashed line.

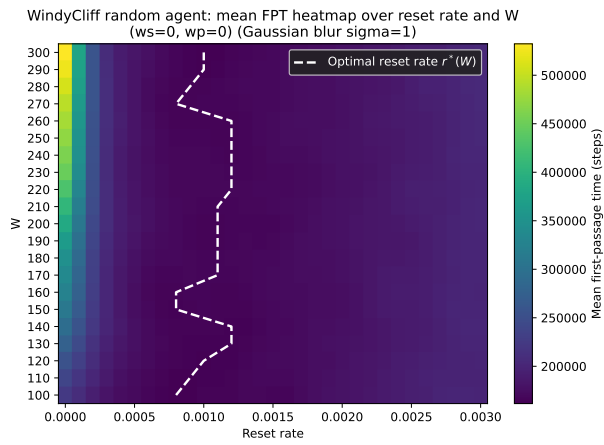
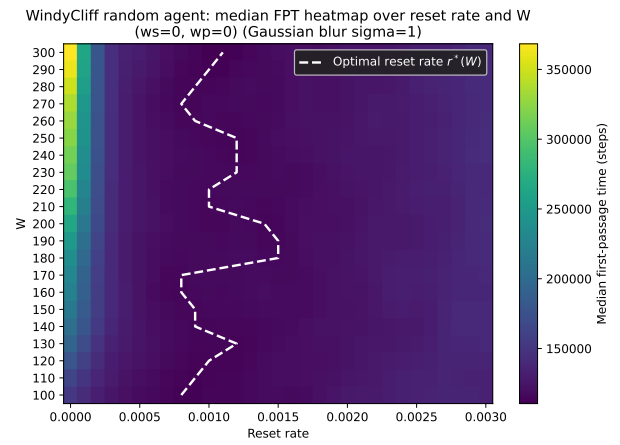
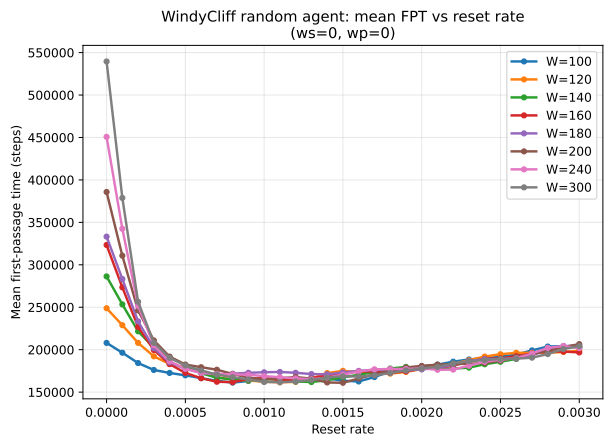
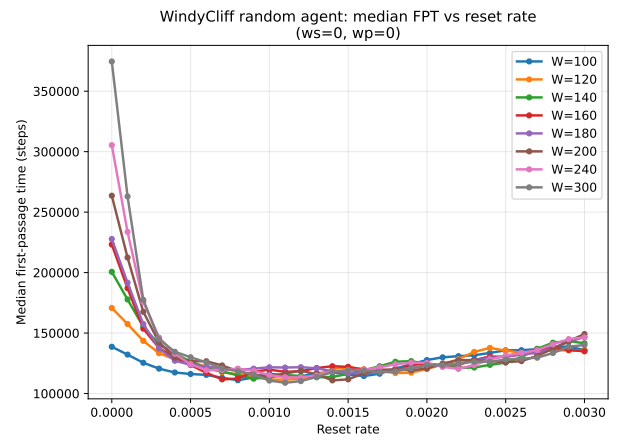
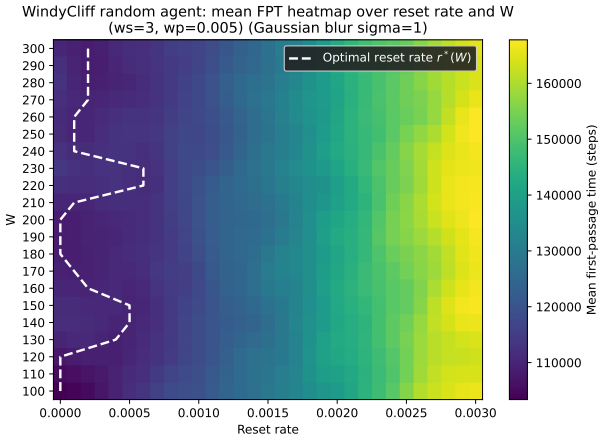
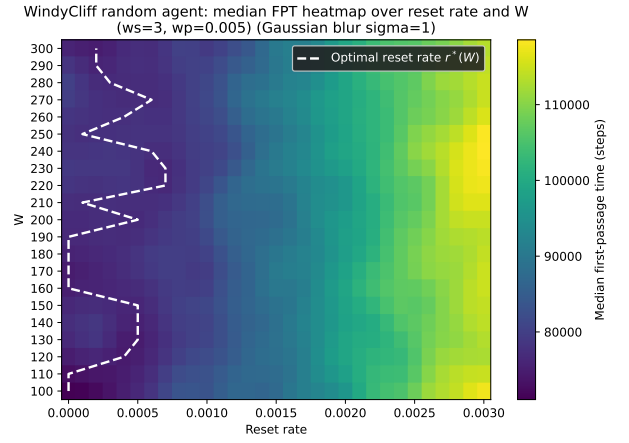
(a) $p_w = 0, s_w = 0$, mean(b) $p_w = 0, s_w = 0$, median(c) $p_w = 0, s_w = 0$, mean(d) $p_w = 0, s_w = 0$, median

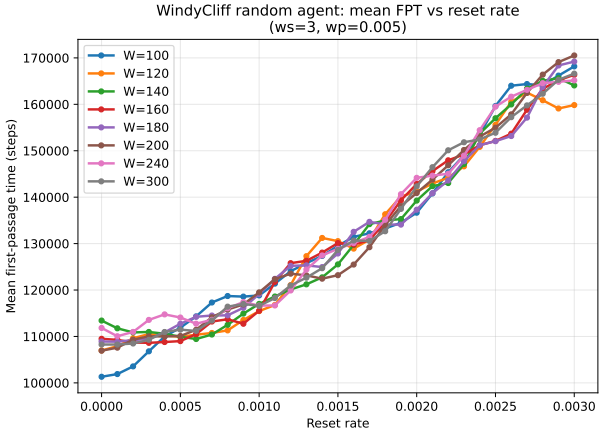
FIG. 8. Mean and median first-passage time in the cliff environment without wind, across different widths and for $H = W/2$, measured over 1000 trials. Displayed here are heatmaps for (a) mean and (b) median FPT, with the optimal resetting rate r^* that minimizes FPT displayed. First-passage time curves for (c) mean and (d) median data is for selected W are also displayed.



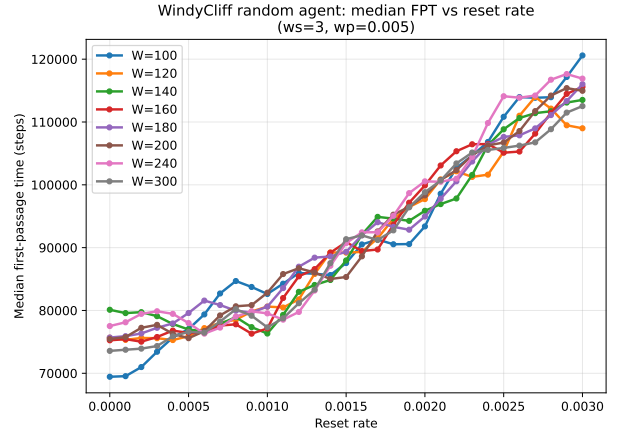
(a) $p_w = 0.005, s_w = 3$, mean



(b) $p_w = 0.005, s_w = 3$, median



(c) $p_w = 0.005, s_w = 3$, mean



(d) $p_w = 0.005, s_w = 3$, median

FIG. 9. Mean and median first-passage time in our Main Text WindyCliff environment: $p_w = 0.005$ and $s_w = 3$, across different widths and for $H = W/2$, measured over 1000 trials. Displayed here are heatmaps for (a) mean and (b) median FPT, with the optimal resetting rate r^* that minimizes FPT displayed. First-passage time curves for (c) mean and (d) median data is for selected W are also displayed.

B. Supporting figures for learning dynamics

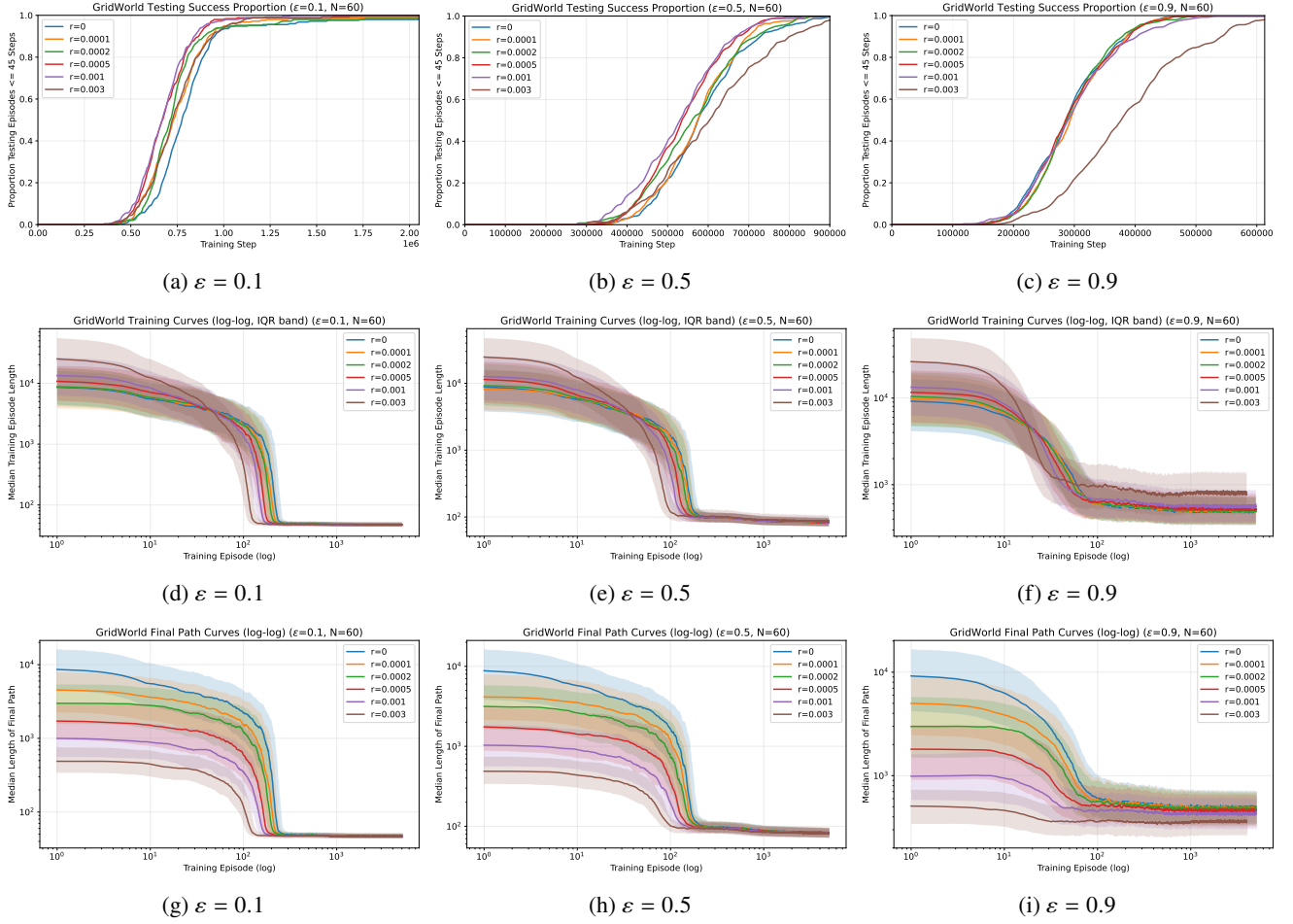


FIG. 10. Extended GridWorld results for $N = 60$. Top row: proportion of testing episodes with length shorter than 45 steps (near-optimal policy; minimum path length 40). Middle row: median training episode lengths with shaded 25-75% quartiles. Bottom row: final path lengths between the start and goal after the last per-episode reset. Each panel shows results for six selected reset rates across ϵ values.

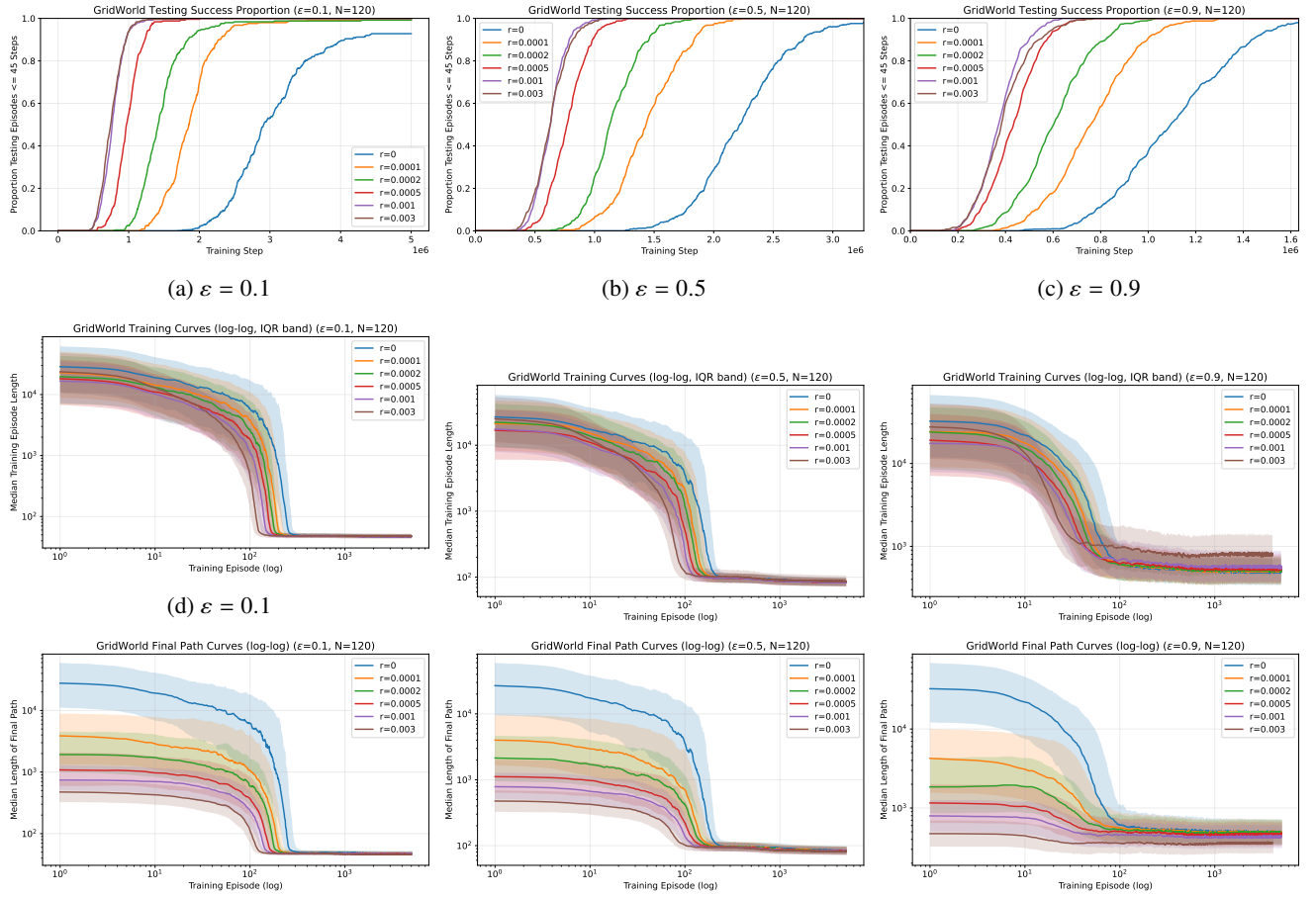


FIG. 11. Extended GridWorld results for $N = 120$. Top row: proportion of testing episodes with length shorter than 45 steps (near-optimal policy; minimum path length 40). Middle row: median training episode lengths with shaded 25–75% quartiles. Bottom row: final path lengths between the start and goal after the last per-episode reset.

Q-Table Evolution in GridWorld

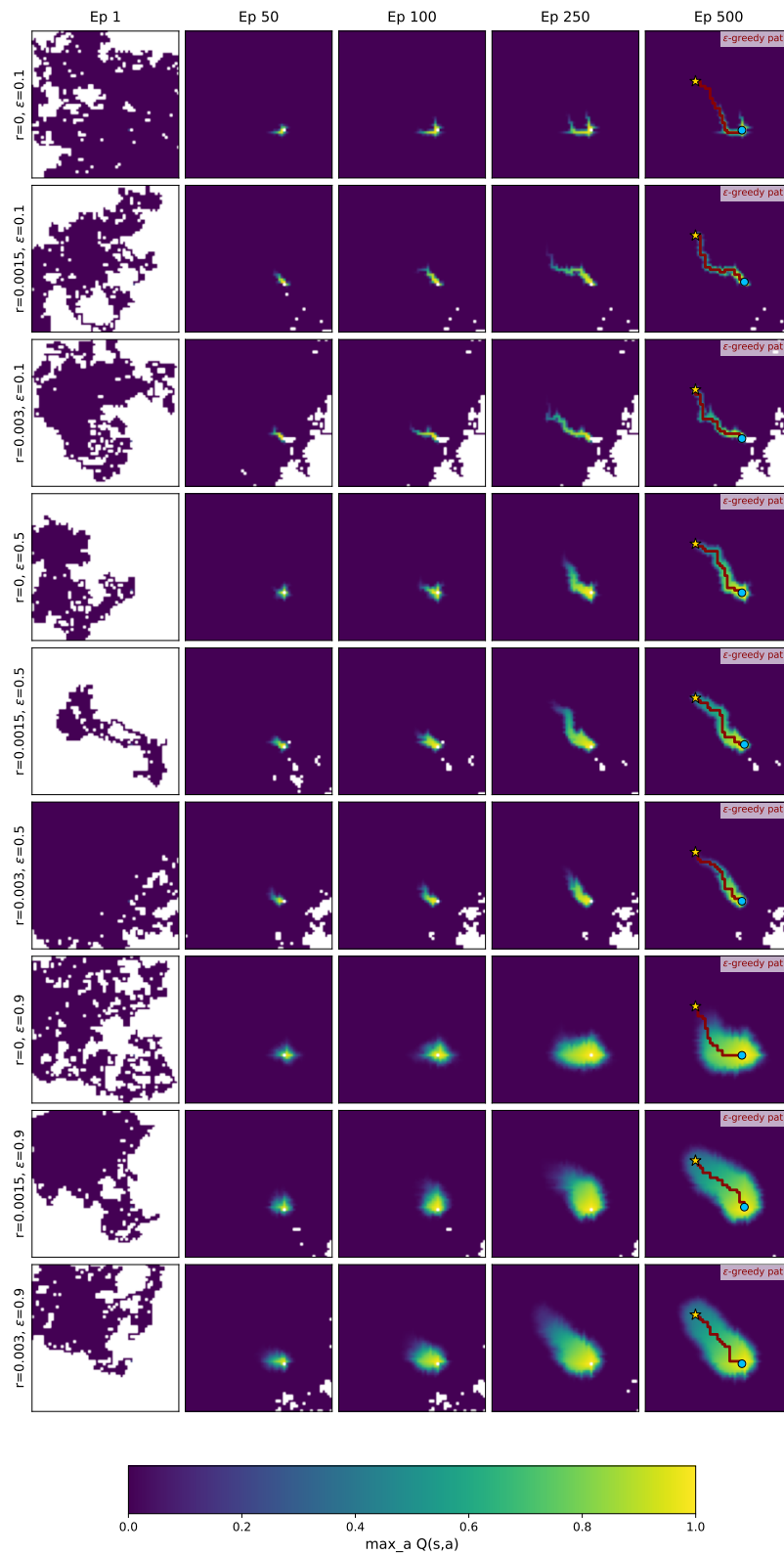


FIG. 12. Snapshots of Q-tables in 60×60 GridWorld, at the end of training episodes 1, 50, 100, 250 and 500. Snapshots plotted for reset rates $r = 0, 0.0015$ and 0.003 and exploration rates $\epsilon = 0.1, 0.5$ and 0.9 . Data plotted is the greedy return at a given state $\max_a Q(s, a)$. White spaces indicate unvisited states. The ϵ -greedy path between the start and goal, determined by the Q-table, is displayed over all episode 500 snapshots.

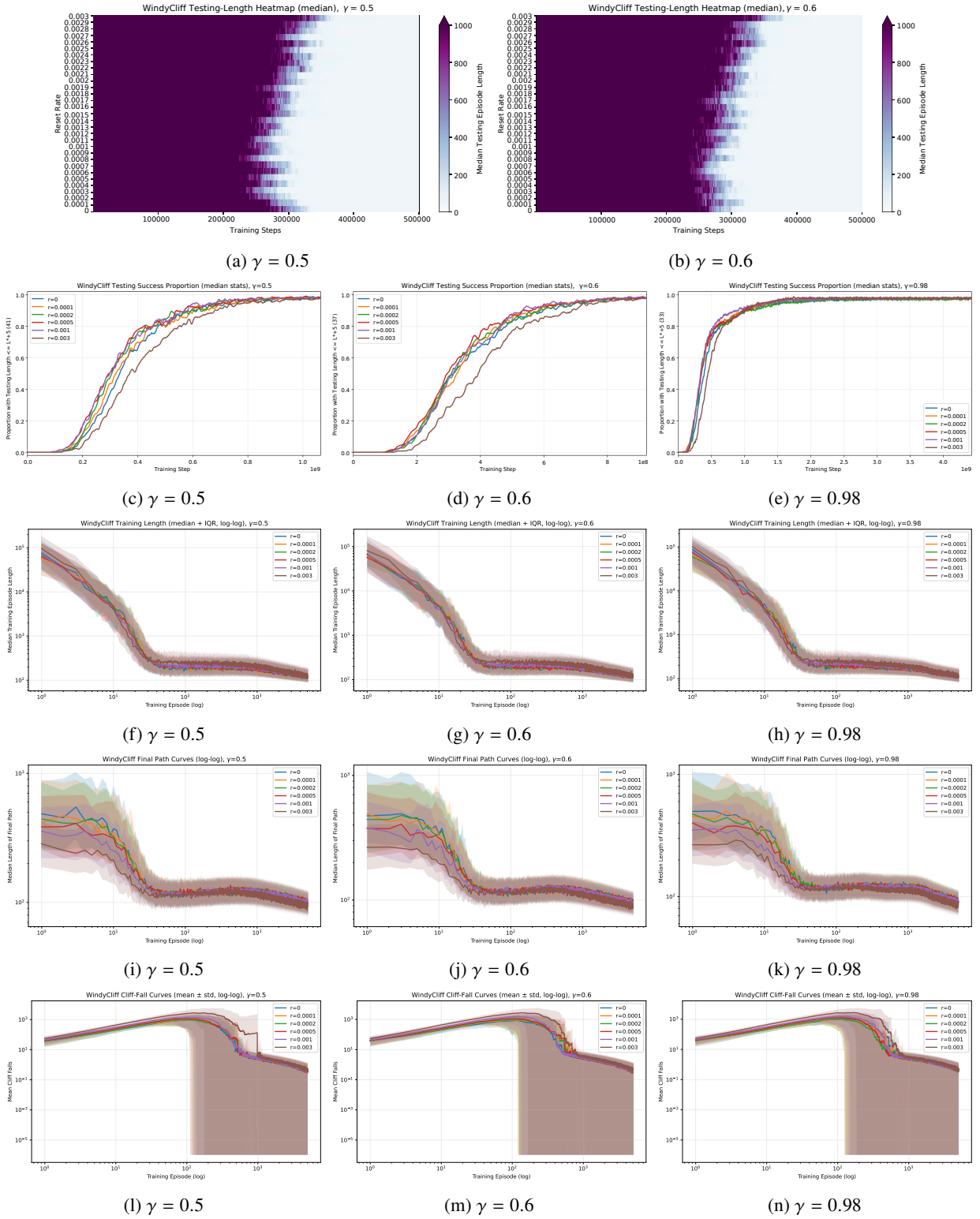


FIG. 13. Extended WindyCliff learning dynamics across discount factors. Top row: heatmaps of median testing episode length across reset rates and training steps for $\gamma = 0.5$ and 0.6 (the $\gamma = 0.98$ case appears in the Main Text, Fig. 3). Second row: proportion of testing episodes with length shorter than $L^* + 5$, indicating near-optimal policies. Third row: median training episode lengths versus episode number. Fourth row: median final contiguous start-goal path lengths during training. Bottom row: mean number of cliff falls per training episode. Parameters tested are $W = 300$, $H = 150$, $p_w = 0.005$, and $s_w = 3$. The optimal path length L^* is determined by dynamic programming (Fig. 6). Shaded regions indicate variability across runs (IQR bands for median and standard deviations for mean).

Q-Table Snapshots in WindyCliff

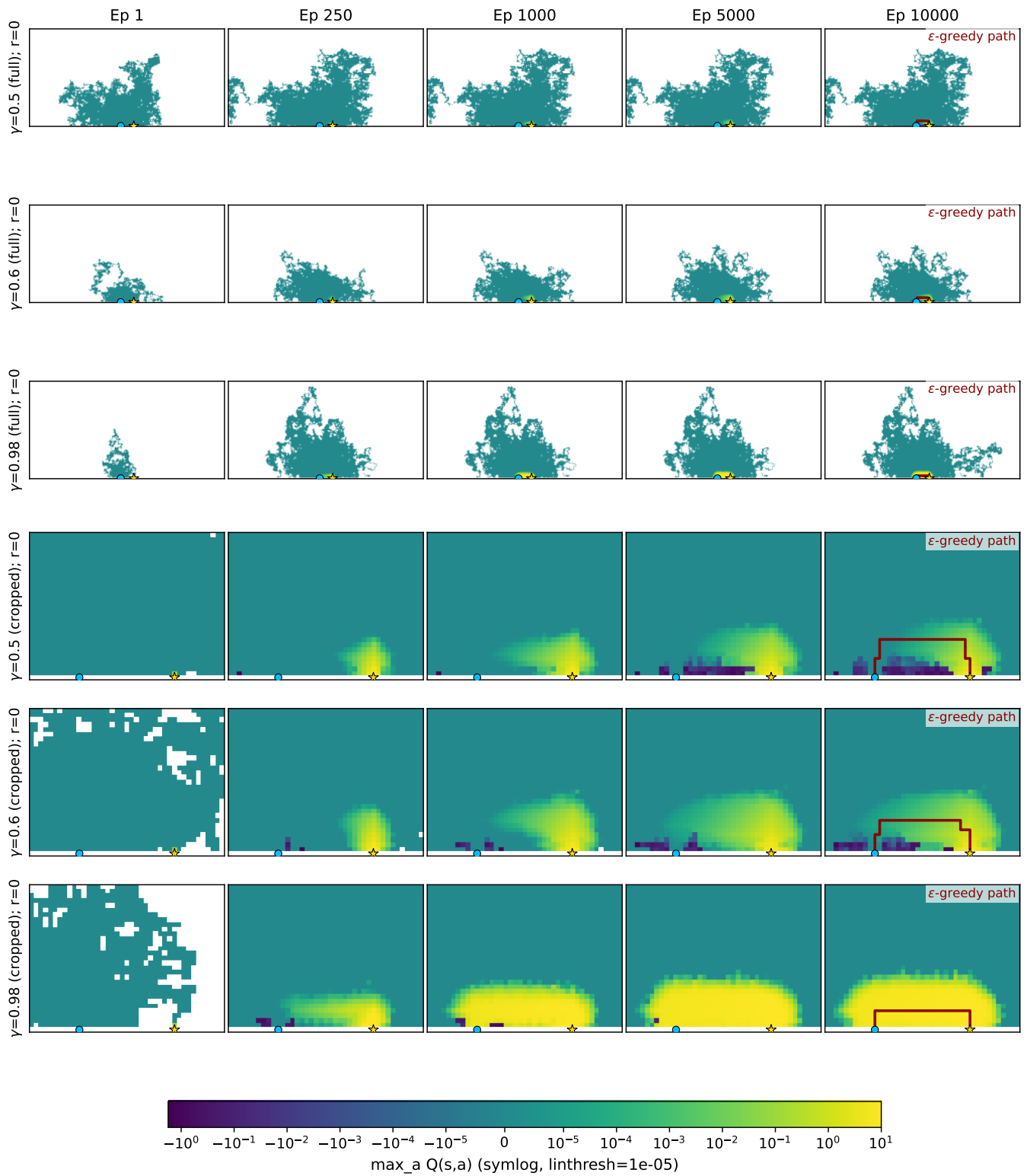


FIG. 14. Heatmaps representing snapshots of $\max_a Q(s, a)$ at selected episode numbers throughout training and with the ϵ -greedy path displayed at the final snapshot. Colour bar displayed in log scale; values bounded at a minimum 10^{-5} to avoid singularities near zero.

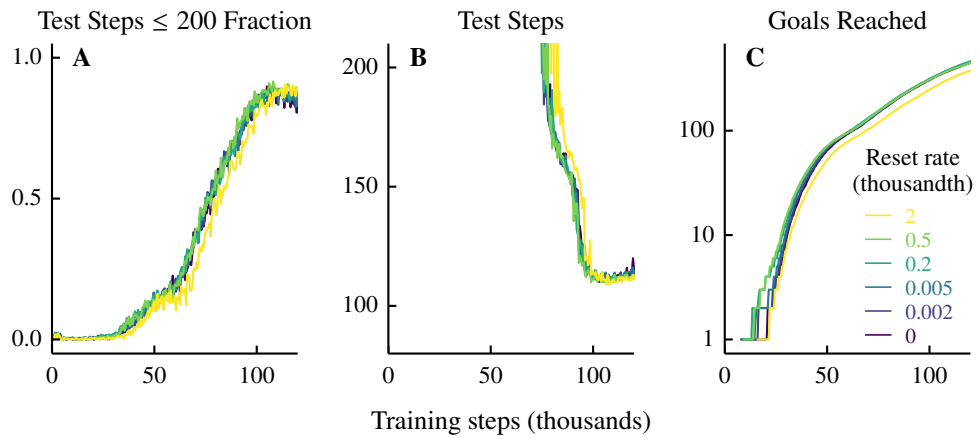


FIG. 15. Same as Fig. 4B–D but for the extended environment (-1.7 left boundary) with the step penalty reward scheme. Learning curves for different reset rates largely overlap; the largest rates modestly impair performance.

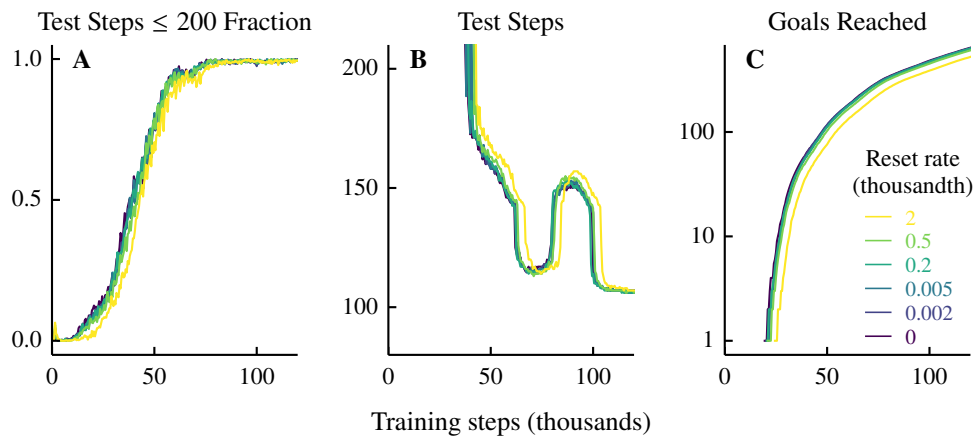


FIG. 16. Same as Fig. 4B–D but for the standard environment (-1.2 left boundary) with the sparse positive reward scheme.

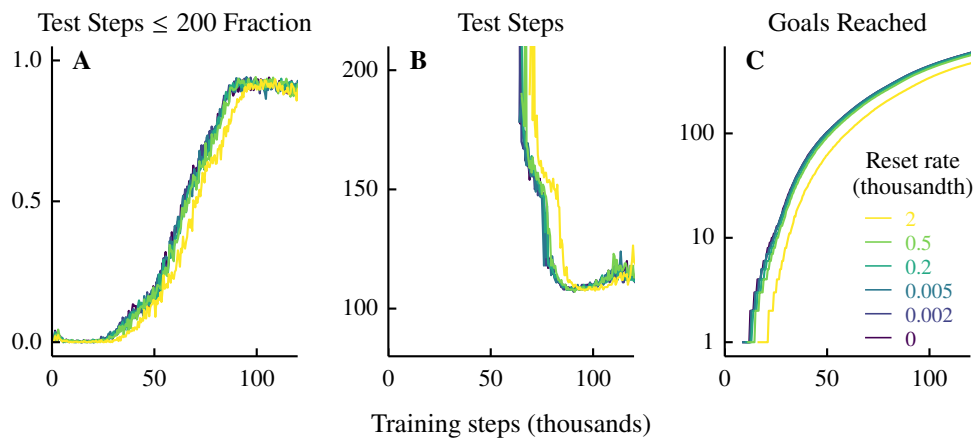


FIG. 17. Same as Fig. 4B–D but for the standard environment (-1.2 left boundary) with the step penalty reward scheme.